

# Journal of Biomedical Optics

BiomedicalOptics.SPIEDigitalLibrary.org

## ***In vivo*, noninvasive functional measurements of bone sarcoma using diffuse optical spectroscopic imaging**

Hannah M. Peterson  
Bang H. Hoang  
David Geller  
Rui Yang  
Richard Gorlick  
Jeremy Berger  
Janet Tingling  
Michael Roth  
Jonathon Gill  
Darren Roblyer

Hannah M. Peterson, Bang H. Hoang, David Geller, Rui Yang, Richard Gorlick, Jeremy Berger, Janet Tingling, Michael Roth, Jonathon Gill, Darren Roblyer, "*In vivo*, noninvasive functional measurements of bone sarcoma using diffuse optical spectroscopic imaging," *J. Biomed. Opt.* **22**(12), 121612 (2017), doi: 10.1117/1.JBO.22.12.121612.

**SPIE.**

# *In vivo*, noninvasive functional measurements of bone sarcoma using diffuse optical spectroscopic imaging

Hannah M. Peterson,<sup>a</sup> Bang H. Hoang,<sup>b</sup> David Geller,<sup>b</sup> Rui Yang,<sup>b</sup> Richard Gorlick,<sup>c</sup> Jeremy Berger,<sup>b</sup> Janet Tingling,<sup>b</sup> Michael Roth,<sup>d</sup> Jonathon Gill,<sup>d</sup> and Darren Roblyer<sup>a,\*</sup>

<sup>a</sup>Boston University, Department of Biomedical Engineering, Boston, Massachusetts, United States

<sup>b</sup>Monefiore Medical Center, Department of Orthopaedic Surgery, Bronx, New York, United States

<sup>c</sup>MD Anderson Cancer Center, Division of Pediatrics, Houston, Texas, United States

<sup>d</sup>Monefiore Medical Center, Department of Pediatrics, Bronx, New York, United States

**Abstract.** Diffuse optical spectroscopic imaging (DOSI) is an emerging near-infrared imaging technique that noninvasively measures quantitative functional information in thick tissue. This study aimed to assess the feasibility of using DOSI to measure optical contrast from bone sarcomas. These tumors are rare and pose technical and practical challenges for DOSI measurements due to the varied anatomic locations and tissue depths of presentation. Six subjects were enrolled in the study. One subject was unable to be measured due to tissue contact sensitivity. For the five remaining subjects, the signal-to-noise ratio, imaging depth, optical properties, and quantitative tissue concentrations of oxyhemoglobin, deoxyhemoglobin, water, and lipids from tumor and contralateral normal tissues were assessed. Statistical differences between tumor and contralateral normal tissue were found in chromophore concentrations and optical properties for four subjects. Low signal-to-noise was encountered during several subject's measurements, suggesting increased detector sensitivity will help to optimize DOSI for this patient population going forward. This study demonstrates that DOSI is capable of measuring optical properties and obtaining functional information in bone sarcomas. In the future, DOSI may provide a means to stratify treatment groups and monitor chemotherapy response for this disease. © 2017 Society of Photo-Optical Instrumentation Engineers (SPIE) [DOI: 10.1117/1.JBO.22.12.121612]

Keywords: *in vivo* imaging; near-infrared; diffuse optics; tissue spectroscopy; therapeutic monitoring; translational research.

Paper 170376SSR received Jun. 8, 2017; accepted for publication Dec. 5, 2017; published online Dec. 20, 2017.

## 1 Introduction

Sarcomas are malignant tumors of connective tissue, including bone, muscle, and cartilage.<sup>1</sup> Although sarcomas represent only a small portion of cancers in the United States (<1%),<sup>2,3</sup> they comprise 12% of all childhood cancers.<sup>4</sup> Five-year disease-free survival and overall survival for localized disease have remained at ~70% for the last 40 years.<sup>2,3,5-8</sup> Osteosarcoma and Ewing's sarcoma are two of the most common childhood sarcomas and the two most common bone malignancies in children and young adults,<sup>2,5</sup> representing 5% of all pediatric cancers.<sup>4</sup>

Osteosarcomas and Ewing's sarcomas are treated as a systemic disease using multiagent neoadjuvant (presurgical) chemotherapy followed by local control and postoperative chemotherapy.<sup>9-11</sup> Currently, there are no methods to determine which sarcoma patients would benefit most from neoadjuvant therapy or immediate surgery. In patients with localized disease, the only clinically accepted prognostic marker to neoadjuvant chemotherapy is histological response.<sup>12</sup> For osteosarcoma and often Ewing's sarcoma, a good histological response is typically defined as having >90% tumor-cell necrosis at the time of surgery, which is correlated with longer disease-free survival, event-free survival, and overall survival rates.<sup>9,10,13,14</sup> Unfortunately, ~40% to 70% of patients have a poor histological response. Additionally, this biomarker can only be determined at the time of surgery, weeks or months after the start of intensive chemotherapy.<sup>15-17</sup> The inability to adequately evaluate

treatment response may contribute to continued poor outcomes,<sup>18</sup> emphasizing the need to identify poor responders early in treatment before surgery.

Other prognostic markers, such as tumor location,<sup>5,10,16</sup> initial tumor size,<sup>12,16</sup> intratumoral microvessel density,<sup>19</sup> disease stage,<sup>5</sup> metastasis,<sup>16</sup> and alkaline phosphatase<sup>10,20-22</sup> have been proposed but remain unverified and are generally not used to guide treatment decisions. Imaging techniques have been mostly unsuccessful in predicting chemotherapy response in sarcoma.<sup>23-25</sup> Volumetric changes may not occur even in responding tumors due to the bony nature of many sarcomas,<sup>24</sup> rendering many structural imaging techniques unhelpful. Diffuse weighted MRI has had mixed results detecting tumor viability, and it remains unverified.<sup>24-27</sup> Recently, the functional imaging techniques FDG PET/CT found that tumor necrosis at the time of diagnosis was correlated with pathologic response and mortality.<sup>28</sup> However, these techniques cannot be used for frequent treatment monitoring because of cost and potential harm to the patient from radiation or exogenous contrast agents.<sup>29</sup> Thus, tumor necrosis at the time of surgery remains the best prognostic marker for sarcoma and finding a new marker earlier in treatment is a priority.<sup>10,16,20,30</sup>

Frequency-domain diffuse optical spectroscopic imaging (DOSI) is a noninvasive imaging technique that can provide tissue molar concentrations of key metabolic and molecular species in thick tissue. DOSI has been studied extensively in the context of breast cancer, where it has been shown that functional hemodynamic information measured using DOSI is correlated

\*Address all correspondence to: Darren Roblyer, E-mail: [roblyer@bu.edu](mailto:roblyer@bu.edu)

with pathologic response as early as the first day after the start of neoadjuvant chemotherapy.<sup>31–33</sup> Similar optical biomarkers may exist in sarcoma. Since DOSI does not rely on structural changes but is sensitive to tumor metabolism and necrosis, it may provide earlier assessments of treatment response than other available methods.

DOSI has not been used previously to evaluate bone sarcomas. These tumors present several challenges due to the varied anatomic locations where they develop, their depth within tissue, and the substantial differences in tissue composition compared with breast tissue. The goals of this work are to establish that sarcomas can be measured in a variety of anatomic locations and to quantify DOSI performance for these measurements, including signal levels and imaging depth. Longitudinal treatment monitoring was not a goal of this study, and measurements were acquired either before or early during treatment. Due to the rarity of this disease, these initial measurements represent a crucial step in laying the groundwork for future studies of this patient population, and point toward improvements in DOSI technology likely needed to achieve optimal results.

## 2 Methods

### 2.1 Diffuse Optical Spectroscopic Imaging Instrumentation

The DOSI system used for this study has been previously described.<sup>34,35</sup> The system is compact and fits on a medical cart, allowing bedside access during chemotherapy. The system acquires both frequency-domain and continuous wave (broadband) measurements. It has a handheld probe that delivers amplitude modulated near-infrared (NIR) light and broadband light to the tissue via 400  $\mu\text{m}$  and 1-mm optical fibers, respectively. Light levels delivered to the tissue are within ANSI limits for skin exposure. For the frequency-domain measurements, light from four lasers (659, 689, 781, and 829 nm) is amplitude modulated in a sweep from 50 to 500 MHz and detected by an avalanche photodiode (APD) with a 0.5-mm active area (C5658 with detector S-6045, Hamamatsu Photonics, Hamamatsu, Japan), which is embedded in the handheld probe. Broadband light from a tungsten-halogen lamp is detected by an NIR spectrometer (650 to 1000 nm). Figure 1 shows a picture of the probe sources and detectors. All measurements for this study were taken with a source–detector separation of 28 mm.

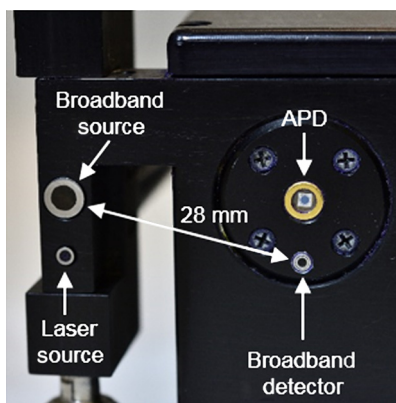


**Fig. 1** Picture of broadband source and detector fibers, laser source fiber bundle, and APD. The region of the probe shown is placed in direct contact with subject's skin during clinical measurements.

### 2.2 Subject Eligibility and Enrollment

All subjects currently diagnosed with a bone sarcoma and scheduled to undergo neoadjuvant chemotherapy were eligible. Informed consent was obtained from all subjects. Minors (<18 years) gave assent to the best of their ability to understand, and their parent or guardian gave written informed consent. This project was approved by the Institutional Review Boards at Boston University and Montefiore Medical Center.

### 2.3 Imaging Procedures

A standard DOSI measurement procedure originally developed for breast and used for several prior published studies was modified for measurements taken in this study.<sup>33,34</sup> A grid of fiducial markers with 1-cm spacing was transferred onto the skin surface overlying or immediately adjacent to the underlying tumor using a transparency and nonpermanent surgical marker. The transparency included distinguishing features, which serve as a reference, such as freckles, moles, scars, and bone landmarks. The landmarks helped to identify the same region of interest for subsequent measurements and to identify the DOSI measurement location on the MRI. An operator scanned the handheld probe over the grid, taking a point measurement at each location. A single point measurement typically took 15 to 30 s, which includes the time it takes to position the probe, ensure good contact between the probe and the skin, and acquire data. After processing the data, a 2-D map of chromophore values is created by a linear interpolation between measurement points. A typical measurement area for this study contained an average of 43 individual point measurements on both the tumor and on the contralateral normal tissue.

### 2.4 Analysis

DOSI measures broadband absorption by combining frequency-domain and continuous wave measurements. Absorption and reduced scattering coefficients ( $\mu_a$  and  $\mu'_s$ , respectively) are calculated from fitting calibrated frequency-domain amplitude and phase measurements from 50 to 400 MHz to the P1 diffusion approximation of the radiative transport equation, assuming a homogenous, semi-infinite media.<sup>36,37</sup> Broadband absorption is fit and scaled to the frequency-domain absorption measurements.<sup>37–39</sup> Using the broadband absorption and known extinction coefficients,<sup>40–43</sup> quantitative concentrations of oxyhemoglobin, deoxyhemoglobin, water, and lipids are calculated using Beer's Law. The Mann–Whitney test was used to statically compare the distribution of point measurements for tumor and contralateral normal tissue using SciPy 0.18.0 in Python version 2.7.9.<sup>44,45</sup>

### 2.5 Estimates of Imaging Depth and Signal-to-Noise Ratio

All subjects had at least one MRI before the start of treatment. A bone landmark near the DOSI measurement site, clearly identifiable by the operator during the DOSI measurement as well as on the corresponding MRI, was used to correlate DOSI measurement regions on the patient's MRI. More specifically, the distance from a bone landmark to a specific DOSI measurement location was recorded on the DOSI transparency. Using the subject's most recent MRI, this distance was measured from the same bone landmark along the surface of the skin using the ruler tool in Centricity Enterprise Web (General Electric

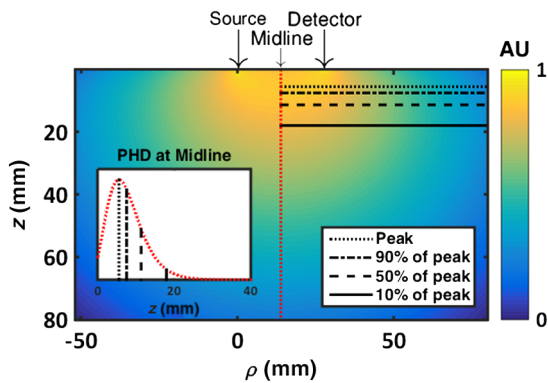


**Fig. 2** DOSI imaging depth estimates from the PHD. At a line perpendicular to the tissue surface emanating from the geometric midpoint between the source and detector locations (red dotted line), the peak PHD (black dotted), and the 90%, 50%, and 10% of the peak PHD (black dash-dot, dashed, and solid lines, respectively) are calculated. The inset shows the PHD profile along the midline.

Company, Chicago, Illinois). Once the DOSI measurement location was found on the MRI, the ruler tool was used to measure the distance perpendicular from the surface of the skin to the edge of the tumor margin, providing an estimate of tumor depth.

DOSI imaging depth was estimated from the photon hitting density (PHD) determined at a line perpendicular to the tissue surface emanating from the geometric midpoint between the source and detector locations. The peak PHD and the 90%, 50%, and 10% of the peak PHD are also recorded. A visual representation of the imaging depths is shown in Fig. 2. The PHD was calculated based on the definition described by Schotland et al.,<sup>46</sup> using the Virtual Photonics Simulator (Virtual Photonics Initiative, Irvine, California) with the analytic solution to the standard diffusion approximation and assuming a homogenous media and an isotropic point source. Simulation optical properties were determined from the optical properties at 689 nm of a DOSI measurement that was colocated with MRI for each subject.

The experimental signal-to-noise ratio (SNR) was calculated as the raw amplitude divided by a dark measurement. The dark measurement was calculated as the average of five measurements taken on a highly absorbing black phantom. For each subject, the median SNR and 10 to 90 percentile range is reported. SNR was calculated as the average SNR for all measurements as a function of the modulation frequency. To be included in the dataset, the 90th percentile of the SNR must be greater than or equal to 3 for three of the four lasers. It was determined that under this threshold, data were not of sufficient quality for accurate optical property extraction. This requirement ensures that there are at least three data points for the power law fit of  $\mu_s'$ . If the SNR did not meet this condition, the subject was excluded from analysis.

### 3 Results

#### 3.1 Enrollment and Tumor Characteristics

Six subjects diagnosed with osteosarcoma ( $n = 4$ ) or Ewing's sarcoma ( $n = 2$ ) were enrolled in the study. Subjects are identified in this manuscript with a four-digit identifier, the first being designated as 1001, the second as 1002, etc. The subject and tumor characteristics of the six subjects are shown in Table 1. Locations measured were the femur ( $n = 3$ ), humerus

**Table 1** Subject and tumor characteristics.

Variable	Group		
	Analysis	Excluded	All
Subjects	4	2	6
Age (years)			
Median	15	16	15
Range	10 to 18	14 to 18	10 to 18
Mean	14	17	15
Sex			
Male	3	2	5
Female	1	0	1
Race			
White	2	0	2
Black/African-American	0	2	2
Hispanic	2	0	2
Site			
Trunk	1	0	1
Extremity	3	2	5
Location			
Left	3	0	3
Right	1	2	3
Disease			
Osteosarcoma	2	2	4
Ewing's sarcoma	2	0	2
Median tumor depth (mm)	9.7	7.5	9.6
Percent necrosis (%)			
Median	98	63	96
Range	85 to 99	30 to 95	30 to 99
Mean	95	63	84
Pathologic response			
Good	3	1	4
Poor	1	1	2
Mean number of DOSI data points per side	38	60	43

( $n = 1$ ), tibia ( $n = 1$ ), and ribs ( $n = 1$ ). Two subjects were excluded from analysis. For one subject diagnosed with osteosarcoma of the distal femur, the tumor location was too sensitive to touch and therefore could not be measured with DOSI. For a different subject diagnosed with osteosarcoma of the proximal

tibia, the DOSI signal was determined to be too low for analysis, likely because of a highly attenuating tumor. Of the remaining four subjects, three were measured with DOSI before neoadjuvant chemotherapy and one was measured on the ninth day of treatment. Of the four subjects included in the analysis group, three were determined to have a good pathologic response to neoadjuvant chemotherapy, and one had a poor response.

### 3.2 Imaging Depth and Signal-to-Noise Ratio

The tumor depth for each of the subjects is shown in Table 2. The peak intensity of the PHD halfway between the source and the detector was calculated as 5.8, 5.6, 4.5, and 5.5 mm for subjects 1001, 1002, 1004, and 1006, respectively. As seen in Table 2, the estimated peak intensity of the PHD does not reach the tumor for any of the measured subjects. 50% of the peak PHD was calculated as 12.8, 11.4, 9.8, and 10.8 mm for subjects 1001, 1002, 1004, and 1006, respectively. 50% of the peak PHD reaches the tumor for subjects 1001 and 1002. For subject 1004, the 50% of the peak PHD is beyond the layer of subcutaneous fat but not within the tumor. However, for three of the four tumors included in the analysis group, 10% of the peak PHD reached the tumor, suggesting some photons are probing the tumor tissue. For subject 1006, the depth at 10% of the peak PHD is within the subcutaneous fat layer.

For subjects 1004 and 1006, poor SNR was achieved at higher modulation frequencies so data were processed from 50 to 300 MHz. For all subjects, the frequency-domain data taken at the shortest wavelength, 659 nm, had the lowest SNR while data taken at 781 nm had the highest SNR, as seen in Table 3. For the frequency-domain data taken at 659 nm, the median SNR and 10 to 90 percentiles for subjects 1001, 1002, 1004, 1005, and 1006 were 82 [29, 149], 41 [13, 68], 9 [3, 11], 2 [1, 2], and 6 [3, 8], respectively. The median SNR taken at 781 nm was 296 [119, 441], 165 [71, 247], 58 [41, 68], 16 [11, 20], and 59 [38, 74], respectively, for subjects 1001, 1002, 1004, 1005, and 1006.

**Table 2** Tumor and imaging depths.

Variable	Subject					
	1001	1002	1003	1004	1005	1006
Tumor depth (mm)	5.89	9.40	9.85	9.99	5.15	32.23
Subcutaneous fat thickness (mm)	5.89	5.7	4.46	4.64	5.15	25.04
Imaging depth (mm)						
Peak PHD intensity	5.8	5.6	<sup>a</sup>	4.5	<sup>b</sup>	5.5
90% of the peak PHD	8.20	7.60	<sup>a</sup>	6.3	<sup>b</sup>	7.4
50% of the peak PHD	12.80	11.40	<sup>a</sup>	9.80	<sup>b</sup>	10.8
10% of the peak PHD	21.40	18.00	<sup>a</sup>	15.5	<sup>b</sup>	16.6

<sup>a</sup>DOSI measurement not taken.

<sup>b</sup>DOSI measurement not processed.

### 3.3 Optical Properties

Optical properties were compared for measurements taken on the tumor and contralateral normal tissues for each subject (Fig. 3). The median and interquartile ranges in Fig. 3 show a high degree of variability between subjects and within subjects, and the shape of the absorption and the reduced scattering coefficient spectra differ substantially among subjects. Among subjects, the differences in absorption magnitude may be caused by differences in intrinsic properties, tumor size, or tumor depth. Within subjects, there are clear differences between tumor and contralateral normal tissues, especially in subjects 1001 and 1004 [Figs. 3(a) and 3(c), respectively]. Subjects 1002 and 1006 have subtle spectral differences between tumor and normal tissue, with the strongest differences appearing in absorption spectra near 980 nm.

There are statistical differences between tumor and contralateral normal scattering amplitude for subject 1001 ( $p = 0.001$ ) and scattering slope for subjects 1001 and 1004 ( $p < 0.001$  and  $p = 0.026$ , respectively). In subjects 1002 and 1006, the scattering amplitude and slope are not statistically different ( $p = 0.26$  and  $p = 0.34$  for subject 1002,  $p = 0.42$  and  $p = 0.44$  for subject 1006). Subjects 1002 and 1006 both have osteosarcoma of the distal femur.

### 3.4 Chromophore Concentrations

There are differences in chromophore concentrations between tumor and contralateral tissue for all subjects in the analysis group. For example, Fig. 4 shows a DOSI measurement of subject 1002 taken prior to neoadjuvant treatment. The measurement area, shown in Fig. 4(a), was a T shape with a 1-cm spaced grid containing 48 points that covered a 7- $\times$ -7-cm area. For this region of interest, the total DOSI measurement time was 24 min. Despite the fact that 50% of the peak PHD did not reach the tumor (Table 2), oxygen saturation maps reveal differences between normal and affected tissue, as seen in Fig. 4(b) ( $p < 0.001$ ). There is a strong visible correlation between oxygen saturation and tumor location, especially at the most superficial bone locations.

Chromophore information is summarized for each subject analyzed in Fig. 5. As shown in Figs. 5(a)–5(d), tumor and contralateral normal tissue statistically differed in total hemoglobin concentration for three of the four subjects ( $p < 0.001$ ,  $p < 0.001$ , and  $p = 0.018$ , for subjects 1001, 1004, and 1006, respectively). Subjects 1002 and 1004 had a higher median total hemoglobin concentration in the tumor compared with the contralateral normal, whereas subjects 1001 and 1006 had the opposite trend. For subject 1001, differences in total hemoglobin were driven by deoxyhemoglobin ( $p < 0.001$ ). For subjects 1004 and 1006, both deoxyhemoglobin ( $p < 0.001$  and  $p = 0.018$ , respectively) and oxyhemoglobin ( $p = 0.003$  and  $p = 0.018$ , respectively) contributed to differences in total hemoglobin concentration. Subject 1002 have a statistically higher oxyhemoglobin concentration in the tumor compared with the contralateral normal tissue ( $p < 0.038$ ).

Oxygen saturation was higher in the tumor compared with the contralateral normal tissue for subjects 1001 and 1002 ( $p < 0.001$  for both). For subject 1006, oxygen saturation is lower in the tumor ( $p = 0.028$ ). At the end of neoadjuvant treatment, these three subjects also had a good response to treatment (>90% tumor-cell necrosis).

**Table 3** Median SNR with 10 to 90 percentiles.

Wavelength (nm)	Subject				
	1001	1002	1004	1005	1006
659	82 [29, 149]	41 [13, 68]	9 [3, 11]	2 [1, 2]	6 [3, 8]
689	89 [37, 152]	44 [18, 75]	13 [9, 17]	3 [2, 3]	10 [6, 13]
781	296 [119, 441]	165 [71, 247]	58 [41, 68]	16 [11, 20]	59 [38, 74]
829	162 [56, 390]	108 [37, 233]	41 [21, 67]	15 [8, 26]	46 [23, 81]

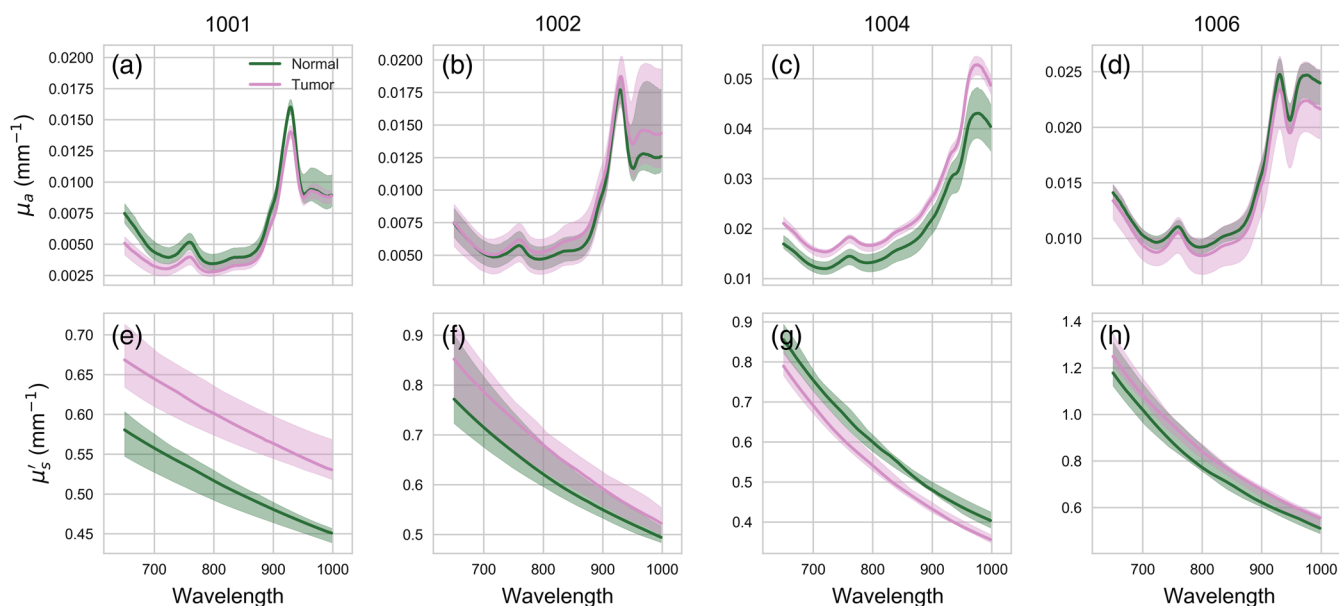


**Fig. 3** Median (solid line) and interquartile range (shaded) of absorption (a to d) and scattering (e to h) coefficients versus source wavelength obtained at tumor (pink) and contralateral normal (green) locations for four sarcoma patients.

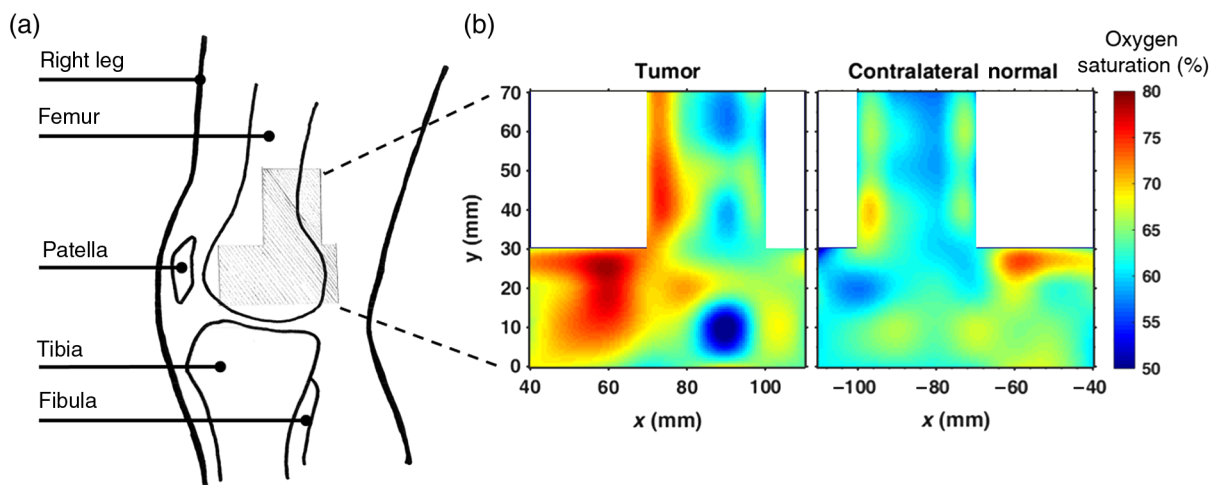


**Fig. 4** A 10-year-old male with osteosarcoma in the right distal femur was measured with DOSI before neoadjuvant chemotherapy. (a) Diagram of bones in the right knee. The measurement area is the shaded region with the origin being the bottom tip of the patella. (b) Oxygen saturation maps for tumor and contralateral normal tissue.

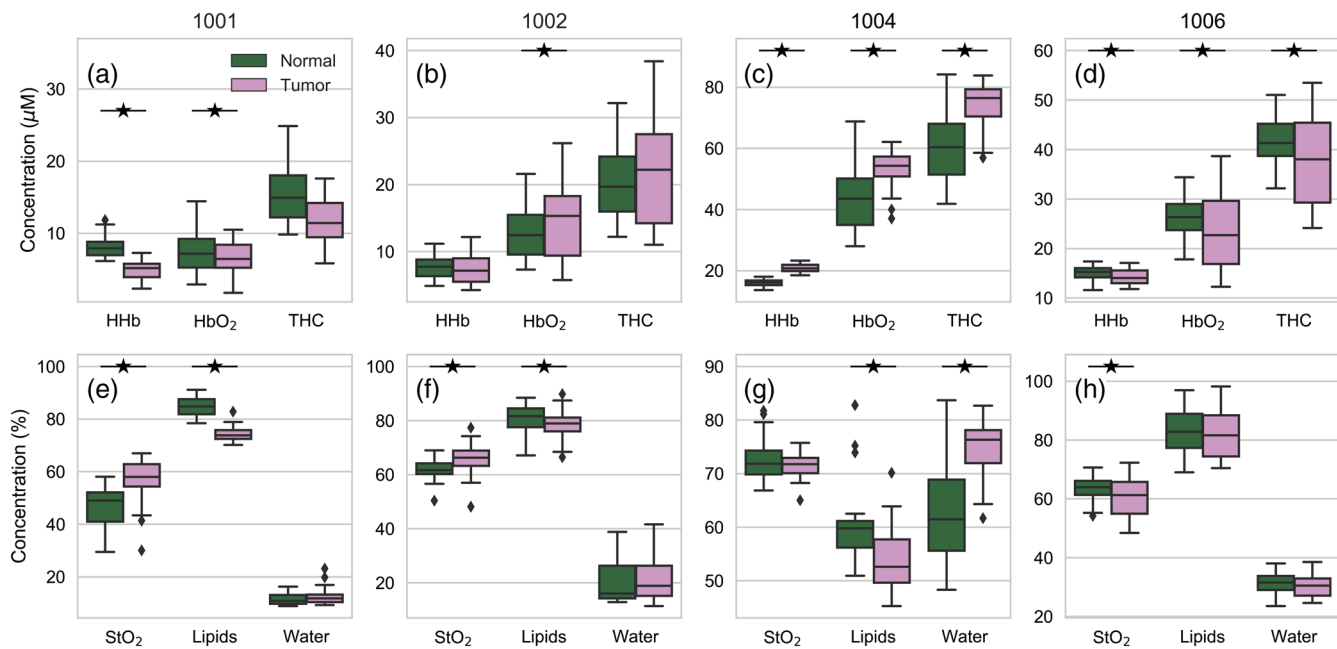


**Fig. 5** Hemoglobin ( $\mu\text{M}$  concentration for panels a to d) and water, lipid, and oxygen saturation (% concentration for panels e to h) for tumor (pink) and contralateral normal (green) tissue for four sarcoma subjects. \* represent a statistical significance between tumor and contralateral normal tissue at  $p = 0.05$ .

As seen in Figs. 5(e) to 5(h), lipid concentrations were lower in tumor tissue compared with contralateral normal tissue for three of the four subjects ( $p < 0.001$ ,  $p = 0.008$ , and  $p < 0.001$  for subjects 1001, 1002, and 1004, respectively). Water concentrations varied greatly among subjects [Figs. 5(e) to 5(h)]. The median water concentration was higher in tumor tissue compared with contralateral normal tissue for all except subject 1006. However, only subject 1004 had a statistical difference in water concentration ( $p < 0.001$ ). Subject 1004 also had a substantially higher water concentration in both tumor and normal tissue compared with the other subjects.

The tissue optical index (TOI) is a commonly used contrast function in DOSI breast cancer measurements.<sup>34,47</sup> TOI is defined as deoxyhemoglobin\*water/lipids, it has been used to identify tumor location.<sup>47</sup> For subjects 1001 and 1004, the TOI is statistically different between tumor and contralateral normal tissue ( $p < 0.001$  for both subjects). This difference in TOI is not present for subjects 1002 and 1006.

#### 4 Discussion

This feasibility study presents, to the best of our knowledge, the first measurements of optical properties and chromophore concentrations of bone sarcomas using DOSI. In two of the six enrolled subjects, DOSI measurements could not be taken due to touch sensitivity ( $n = 1$ ) or could not be analyzed due to high tissue attenuation ( $n = 1$ ). In the remaining four subjects, DOSI measurements demonstrated contrast between tumor and contralateral normal tissue in both optical properties and chromophore concentrations. These results suggest that DOSI is capable of measuring and characterizing sarcoma tumors, although improvements in DOSI probe technology are needed to acquire accurate measurements in a larger portion of this patient population.

The sarcomas measured in this study presented a diverse pattern of chromophore concentrations. Despite this diversity, several commonalities were noted. For example, three of the four subjects had statistically lower lipid concentrations in the tumor

compared with the contralateral normal tissue. Of these, subjects 1001 and 1004 had the largest differences in tumor lipid concentration compared with contralateral normal, and both had Ewing’s sarcoma with a soft tissue component. For these subjects, the tumor may have displaced lipids content as it grew. Subject 1006 also had a soft tissue component; however, there was no discernible difference in lipid concentration between the tumor and contralateral normal side, likely because the tumor was so deep (33.23 mm below the skin surface). It is also of note that the extracted lipid concentrations for subjects 1001, 1002, and 1006 are higher than those previously reported for bony locations on the limbs, although these prior reports were from more superficial locations.<sup>48,49</sup>

While lipids were generally different in tumor compared with contralateral normal regions, only subject 1004 had significantly different water concentrations between tumor and contralateral normal tissue. It is of note that the magnitude of the water concentration for subject 1004 was much greater than the other subjects, and subject 1004 had the only measurement location not on the limbs (the tumor was on the ribs). Literature values for water concentrations in tissue vary greatly<sup>48–50</sup> but with the exception of subject 1004, the water concentrations in this study are similar to those previously reported for other bony locations on the limbs.<sup>48</sup>

Hemoglobin levels varied to a large extent over subjects, but the concentrations of oxyhemoglobin and deoxyhemoglobin are generally comparable with other literature values for bony tissue.<sup>48,49,51–53</sup> Median oxygen saturation values ranged from ~50% to 70%, which fall on the low end of values reported in literature for other diffuse measurements performed on bone [Figs. 5(e)–5(h)].<sup>48,51,54</sup> It is of note that the bone measurements in this study were not as superficial nor from the same locations as those in literature.

An interesting result from this study is that subjects 1001 and 1002 had a higher oxygen saturation in the tumor compared with the contralateral normal tissue. Higher oxygen saturation could

be from shunting or the increased metabolic demand of the tumor.<sup>55</sup> As a static measurement, DOSI cannot distinguish differences between oxygen delivery and consumption, but adding a measure of blood flow may shed light on the specific physiology of these tumors.<sup>56</sup>

The TOI showed contrast between tumor and contralateral normal tissue for the subjects with Ewing's sarcoma. Both of these subjects had a soft tissue component that was more superficial to the surface of the skin. The subjects without TOI contrast had osteosarcoma of the distal femur.

#### 4.1 Limitations

There were several notable limitations of this study. First, due largely to the rarity of the disease, the number of subjects is small and the anatomic sites measured are diverse. For these reasons, the data shown serve as the first documentation of the optical characterization of this patient population, but it is not possible to make generalized statements about sarcoma optical properties and chromophore concentrations without more data.

The next potential limitation includes the choice of chromophores for this study. For this investigation, oxyhemoglobin, deoxyhemoglobin, water, and lipids were fit to measured broadband absorption spectra. Collagen is also an important component in bone, tendon, cartilage, muscle, and skin,<sup>57</sup> and several groups have added collagen to their fitting procedures.<sup>48–50,52,58</sup> The use of collagen as a contributing absorber is relatively recent, and there are limited experimental methods to validate the accuracy of collagen fits. For example, there are no known reports demonstrating the fabrication of tissue mimicking optical phantoms that incorporate collagen at physiologically relevant concentrations at the volume scales needed for diffuse optical measurements. These reasons contributed to the decision not to include collagen in this study.

An additional potential limitation involves the use of the specific light propagation model. For this study, the P1 diffusion approximation of the Boltzmann transport equation was used. This model assumes a homogeneous optically diffusive media, and the specific boundary conditions used for solving the analytical diffusion equation assume a semi-infinite media.<sup>36,37</sup> It has not been validated that *in vivo* measurements of bone, which is porous and highly structured, meet these criteria. It is notable that available NIR absorption spectra of bone indicate that reduced scattering is at least an order of magnitude larger than absorption, providing support that bone is an optically diffusive media.<sup>49</sup> *In vivo* measurements; however, involve multiple chromophores, layered tissue, and complex microarchitecture.

#### 4.2 Future Work

Despite several potential limitations of this work, the data indicate that bone sarcomas are amenable to measurement with diffuse optical technologies and that optical contrast exists between tumor and contralateral normal regions. Improvements in instrumentation, including the ability to measure more highly absorbing tissue at deeper imaging depths, will be key to collecting future high-quality data sets. Additionally, investigations into the inclusion of other chromophores (e.g., collagen), further validation of the models used, investigations into the effects of bone optical anisotropy, and improved coregistration with anatomic imaging modalities will assist in validating diffuse optics

as a useful technique in this patient population. We describe several specific technical challenges here.

Imaging depth is a challenge for some bone sarcomas. Photons must travel through skin, subcutaneous lipids, muscle, and bone to reach many of these tumors. For three of the four subjects analyzed in this study, the tumor depth overlapped with imaging depths (Table 2), but in one subject, it is suspected that the tumor was too deep to be measured with the current probe geometry (subject 1006, 32.23 mm below the surface). Based on simulations of PHD for matched optical properties in this region, a source–detector separation of 88 mm would be required for the 10% of the PHD peak to reach the tumor margin, whereas the current probe used a 28-mm source–detector separation. It is possible that the measured differences between tumor and normal tissue for this subject arise from inflammation or other peritumoral effects. To better match tumor and imaging depths for cases like this, increased source–detector separations could be implemented, transmission geometries could be explored, or the use of late-photon gating could be used in time-domain systems to preferentially emphasize the contribution of photons that have traveled more deeply.<sup>59</sup>

Improvements in signal level would greatly assist for measurements in this patient population. Tumors measured in the study had a large range of overall optical attenuation, and for some subjects the measured hemoglobin concentrations were very high (e.g., subject 1004 had an average tumor total hemoglobin level  $>70 \mu\text{M}$ ), presenting a challenge for achieving adequate SNR. In another subject (subject 1005), the SNR was determined to be too low for accurate optical property extractions. Additionally, if a larger source–detector separation were implemented to measure deeper tissues, increased detector sensitivity would also be required to avoid low SNR. To increase the SNR, larger area APDs or photomultiplier tubes (PMTs) could be utilized, but each of these design choices involve trade-offs. For example, larger areas APDs generally have reduced modulation bandwidth, and PMTs have limited dynamic range and linear operating regions.<sup>58</sup>

Improvements to probe geometry and materials would also assist in measuring this patient population. For example, one subject (subject 1003) could not be measured because the tumor region was too tactile sensitive for a contact probe. A smaller probe footprint or different, softer, probe materials may alleviate this, but it is possible that subject tactile sensitivity could be a limitation of the technology for a portion of this patient population. Additionally, while the majority of bone sarcomas form in the long bones of the body<sup>16</sup> sarcomas can form anywhere, and the probe needs to accommodate a wide range of anatomic sites. A smaller probe footprint or a flexible probe geometry may help facilitate measurements on angular and bony surfaces. Additionally, larger source–detector separations may be necessary to access deep tumors.

## 5 Conclusions

This study demonstrated the ability of DOSI to measure optical properties and functional information at several common sarcoma locations. DOSI was able to differentiate between healthy and sarcoma tissue, although there was substantial variation among subjects. Going forward, several key technological developments are required to better measure this patient population, including more flexible probes and more sensitive detection. Additionally, larger datasets are needed to characterize and quantify sarcoma optical properties and treatment response

dynamics. In the future, DOSI may provide a new means to stratify treatments and monitor chemotherapy response in bone sarcomas, positively impacting treatment decisions and patient outcomes.

### Disclosures

The authors have no conflicts of interest.

### Acknowledgments

The authors thank the patients who agreed to participate in the study. The authors gratefully acknowledge funding from the St. Baldrick's Foundation (Research Grant Award ID: 426642). The authors also thank Bruce Tromberg, Amanda Durkin, Anais Leproux, Brian Hill, and Thomas O'Sullivan for their technical assistance during this project. This work was made possible in part by the Laser Microbeam and Medical Program (LAMMP: P41 EB015890-33), an NIH/NIBIB Biotechnology Resource Center.

### References

1. M. J. Klein and G. P. Siegal, "Osteosarcoma: anatomic and histologic variants," *Am. J. Clin. Pathol.* **125**, 555–581 (2006).
2. "SEER cancer statistics factsheets: bone and joint cancer," National Cancer Institute, Bethesda, Maryland, <http://seer.cancer.gov/statfacts/html/bones.html> (6 May 2016).
3. "SEER cancer statistics factsheets: soft tissue including heart cancer," National Cancer Institute, Bethesda, Maryland, <http://seer.cancer.gov/statfacts/html/soft.html> (17 May 2016).
4. N. Howlander et al., "SEER cancer statistics review, 1975–2013," Technical Report, National Cancer Institute, Bethesda, Maryland (2016).
5. L. Mirabello, R. J. Troisi, and S. A. Savage, "Osteosarcoma incidence and survival rates from 1973 to 2004," *Cancer* **115**, 1531–1543 (2009).
6. M. P. Link et al., "The effect of adjuvant chemotherapy on relapse-free survival in patients with osteosarcoma of the extremity," *N. Engl. J. Med.* **314**, 1600–1606 (1986).
7. G. Uribe-Botero et al., "Primary osteosarcoma of bone: a clinicopathologic investigation of 243 cases, with necropsy studies in 54," *Am. J. Clin. Pathol.* **67**, 427–435 (1977).
8. D. C. Dahlin and M. B. Coventry, "Osteogenic sarcoma," *J. Bone Joint Surg.* **49**, 101–110 (1967).
9. H. S. Hosalkar and J. P. Dormans, "Limb sparing surgery for pediatric musculoskeletal tumors," *Pediatr. Blood Cancer* **42**, 295–310 (2004).
10. P. A. Meyers et al., "Chemotherapy for nonmetastatic osteogenic sarcoma: the memorial Sloan–Kettering experience," *J. Clin. Oncol.* **10**, 5–15 (1992).
11. M. V. Mehren et al., "NCCN guidelines soft tissue sarcoma, version 2.2014," *J. Natl. Compr. Cancer Network* **12**, 473–483 (2014).
12. P. Bieling et al., "Tumor size and prognosis in aggressively treated osteosarcoma," *J. Clin. Oncol.* **14**, 848–858 (1996).
13. A. J. Provisor et al., "Treatment of nonmetastatic osteosarcoma of the extremity with preoperative and postoperative chemotherapy: a report from the Children's Cancer Group," *J. Clin. Oncol.* **15**, 76–84 (1997).
14. J. S. Wunder et al., "The histological response to chemotherapy as a predictor of the oncological outcome of operative treatment of Ewing sarcoma," *J. Bone Joint Surg.* **80**, 1020–1033 (1998).
15. E. I. Hauben et al., "Does the histological subtype of high-grade central osteosarcoma influence the response to treatment with chemotherapy and does it affect overall survival? A study on 570 patients of two consecutive trials of the European Osteosarcoma Intergroup," *Eur. J. Cancer* **38**, 1218–1225 (2002).
16. S. S. Bielack et al., "Prognostic factors in high-grade osteosarcoma of the extremities or trunk: an analysis of 1,702 patients treated on neoadjuvant Cooperative Osteosarcoma Study Group protocols," *J. Clin. Oncol.* **20**, 776–790 (2002).
17. G. Bacci et al., "Neoadjuvant chemotherapy for high-grade central osteosarcoma of the extremity," *Cancer* **97**, 3068–3075 (2003).
18. K. Asha, A. Sachin, and S. Muzammil, "Chemotherapy in osteosarcoma," in *Osteosarcoma*, M. Agarwal, Ed., InTech (2012).
19. M. Kreuter et al., "Prognostic relevance of increased angiogenesis in osteosarcoma," *Clin. Cancer Res.* **10**, 8531–8537 (2004).
20. G. Bacci et al., "Adjuvant and neoadjuvant chemotherapy for osteosarcoma of the extremities: 27 year experience at Rizzoli Institute, Italy," *Eur. J. Cancer* **41**, 2836–2845 (2005).
21. A. M. Levine and S. A. Rosenberg, "Alkaline phosphatase levels in osteosarcoma tissue are related to prognosis," *Cancer* **44**, 2291–2293 (1979).
22. G. Bacci et al., "Prognostic factors for osteosarcoma of the extremity treated with neoadjuvant chemotherapy," *Cancer* **106**, 1154–1161 (2006).
23. The ESMO/European Sarcoma Network Working Group, "Bone sarcomas: ESMO clinical practice guidelines for diagnosis, treatment and follow-up," *Ann. Oncol.* **25**, iii113–iii123 (2014).
24. J. Bajpai et al., "Role of MRI in osteosarcoma for evaluation and prediction of chemotherapy response: correlation with histological necrosis," *Pediatr. Radiol.* **41**(4), 441–450 (2011).
25. R. B. Sanchez et al., "Musculoskeletal neoplasms after intraarterial chemotherapy: correlation of MR images with pathologic specimens," *Radiology* **174**, 237–240 (1990).
26. B. A. Moffat et al., "The functional diffusion map: an imaging biomarker for the early prediction of cancer treatment outcome," *Neoplasia* **8**, 259–267 (2006).
27. M. Uhl et al., "Evaluation of tumour necrosis during chemotherapy with diffusion-weighted MR imaging: preliminary results in osteosarcomas," *Pediatr. Radiol.* **36**(12), 1306–1311 (2006).
28. R. Rakheja et al., "Necrosis on FDG PET/CT correlates with prognosis and mortality in sarcomas," *Am. J. Roentgenol.* **201**, 170–177 (2013).
29. K. Facey et al., "Overview of the clinical effectiveness of positron emission tomography imaging in selected cancers," *Health Technol. Assess.* **11** (2007).
30. A. M. Davis, R. S. Bell, and P. J. Goodwin, "Prognostic factors in osteosarcoma: a critical review," *J. Clin. Oncol.* **12**, 423–431 (1994).
31. S. Ueda et al., "Baseline tumor oxygen saturation correlates with a pathologic complete response in breast cancer patients undergoing neoadjuvant chemotherapy," *Cancer Res.* **72**, 4318–4328 (2012).
32. D. Roblyer et al., "Optical imaging of breast cancer oxyhemoglobin flare correlates with neoadjuvant chemotherapy response one day after starting treatment," *Proc. Natl. Acad. Sci. U. S. A.* **108**, 14626–14631 (2011).
33. A. E. Cerussi et al., "Diffuse optical spectroscopic imaging correlates with final pathological response in breast cancer neoadjuvant chemotherapy," *Philos. Trans. R. Soc., A* **369**, 4512–4530 (2011).
34. B. J. Tromberg et al., "Predicting responses to neoadjuvant chemotherapy in breast cancer: ACRIN 6691 trial of diffuse optical spectroscopic imaging," *Cancer Res.* **76**, 5933–5944 (2016).
35. K.-S. No et al., "Design and testing of a miniature broadband frequency domain photon migration instrument," *J. Biomed. Opt.* **13**(5), 050509 (2008).
36. R. C. Haskell et al., "Boundary conditions for the diffusion equation in radiative transfer," *J. Opt. Soc. Am. A* **11**, 2727 (1994).
37. T. H. Pham et al., "Broad bandwidth frequency domain instrument for quantitative tissue optical spectroscopy," *Rev. Sci. Instrum.* **71**, 2500–2513 (2000).
38. F. Bevilacqua et al., "Broadband absorption spectroscopy in turbid media by combined frequency-domain and steady-state methods," *Appl. Opt.* **39**, 6498–6507 (2000).
39. MATLAB 2014a, The MathWorks Inc., Natick, Massachusetts (2014).
40. R. M. Pope and E. S. Fry, "Absorption spectrum (380–700 nm) of pure water. II. Integrating cavity measurements," *Appl. Opt.* **36**, 8710–8723 (1997).
41. L. Kou, D. Labrie, and P. Chylek, "Refractive indices of water and ice in the 0.65- to 2.5- $\mu$ m spectral range," *Appl. Opt.* **32**, 3531–3540 (1993).
42. R. L. P. van Veen et al., "Determination of VIS-NIR absorption coefficients of mammalian fat, with time- and spatially resolved diffuse reflectance and transmission spectroscopy," in *Biomedical Topical Meeting*, paper SF4, Optical Society of America (2004).
43. W. G. Zijlstra, A. Buursma, and O. W. V. Assendelft, *Visible and Near Infrared Absorption Spectra of Human and Animal Haemoglobin: Determination and Application*, VSP, Utrecht (2000).

44. Python Software Foundation, "Python Language Reference," version 2.7, <http://www.python.org> (2015).
45. E. Jones et al., "SciPy: open source scientific tools for Python," 2001, <http://www.scipy.org/> (21 April 2017).
46. J. C. Schotland, J. C. Haselgrove, and J. S. Leigh, "Photon hitting density," *Appl. Opt.* **32**, 448 (1993).
47. A. Cerussi et al., "*In vivo* absorption, scattering, and physiologic properties of 58 malignant breast tumors determined by broadband diffuse optical spectroscopy," *J. Biomed. Opt.* **11**(4), 044005 (2006).
48. S. K. V. Sekar et al., "Time-resolved diffused optical characterization of key tissue constituents of human bony prominence locations," *Proc. SPIE* **9538**, 95380X (2015).
49. A. Pifferi et al., "Optical biopsy of bone tissue: a step toward the diagnosis of bone pathologies," *J. Biomed. Opt.* **9**(3), 474–480 (2004).
50. P. Taroni et al., "Absorption of collagen: effects on the estimate of breast composition and related diagnostic implications," *J. Biomed. Opt.* **12**, 014021 (2007).
51. P. Farzam et al., "Pulsatile and steady-state hemodynamics of the human patella bone by diffuse optical spectroscopy," *Physiol. Meas.* **34**(8), 839–857 (2013).
52. S. K. V. Sekar et al., "Broadband (600–1350 nm) time resolved diffuse optical spectrometer for clinical use," *IEEE J. Sel. Top. Quantum Electron.* **22**(3), 406–414 (2016).
53. R. M. P. Doornbos et al., "The determination of *in vivo* human tissue optical properties and absolute chromophore concentrations using spatially resolved steady-state diffuse reflectance spectroscopy," *Phys. Med. Biol.* **44**(4), 967–981 (1999).
54. P. Farzam et al., "Noninvasive characterization of the healthy human manubrium using diffuse optical spectroscopies," *Physiol. Meas.* **35**(7), 1469–1491 (2014).
55. P. Vaupel, F. Kallinowski, and P. Okunieff, "Blood flow, oxygen and nutrient supply, and metabolic microenvironment of human tumors: a review," *Cancer Res.* **49**, 6449–6465 (1989).
56. J. M. Cochran et al., "Longitudinal optical monitoring of blood flow in breast tumors during neoadjuvant chemotherapy," *Phys. Med. Biol.* **62**(12), 4637–4653 (2017).
57. H. Lodish et al., "Collagen: the fibrous proteins of the matrix," in *Molecular Cell Biology*, W. H. Freeman, Ed., 4th ed., New York (2000).
58. Y. Zhao et al., "Collagen quantification in breast tissue using a 12-wavelength near infrared spectral tomography (NIRST) system," *Biomed. Opt. Express* **8**, 4217–4229 (2017).
59. A. D. Mora et al., "Towards next-generation time-domain diffuse optics for extreme depth penetration and sensitivity," *Biomed. Opt. Express* **6**, 1749–1760 (2015).

**Hannah M. Peterson** is PhD candidate in biomedical engineering at Boston University. She received her BS degree in physics from Rensselaer Polytechnic Institute in 2011 and her MS degree in biomedical engineering from Boston University in 2016. Prior to her graduate career, she was a postbachelor fellow at the Institute for Health Metrics and Evaluation. Her research interests include medical technologies and public health. She is a member of SPIE.

**Janet Tingling** received her BS and MS degrees in biology and her MBA in healthcare management. She is a doctoral candidate in 2018.

**Michael Roth** is an assistant professor in the Division of Pediatric Hematology/Oncology at the Albert Einstein College of Medicine. After receiving his BA degree in biology from Brandeis University in 2002, received his MD from the NYU School of Medicine, in 2006 and subsequently completed training in pediatrics and pediatric hematology/oncology at the Albert Einstein College of Medicine.

**Jonathan Gill** is a practicing pediatric oncologist with a focus in patients with bone and soft tissue sarcomas. He has a particular interest in developmental therapeutics. He is active in clinical trials both in National Cooperative Trials as well as at the local level.

**Darren Roblyer** is an assistant professor of biomedical engineering at Boston University. He received his BS degree in biomedical engineering from Johns Hopkins University in 2004, and received his PhD in bioengineering at Rice University in 2009. He did his postdoctoral work at the Beckman Laser Institute at the University of California, Irvine. He is a senior member of SPIE.

Biographies for the other authors are not available.